ELSEVIER

Chemical Engineering Journal 133 (2007) 69–77

Chemical Engineering Journal

www.elsevier.com/locate/cej

Instability study of a swirling annular liquid sheet of polymer produced by air-blast atomization

Edgar P. Herrero, E.M. Martín Del Valle *, M.A. Galán

Department of Chemical Engineering, University of Salamanca, P/Los Caídos S/N, 37008 Salamanca, Spain

Received 23 June 2006; received in revised form 17 January 2007; accepted 20 January 2007

Abstract

A temporal stability analysis was carried out to model the atomization of a swirling viscous annular liquid sheet emanating from an air-blast atomizer subject to inner and outer inviscid swirling air streams. The dimensionless dispersion equation that governs the instability of a viscous annular liquid sheet under swirling air streams was obtained. Numerical solutions to the dispersion equation under a wide range of flow conditions were obtained to investigate the effect of the liquid and gas flow on the maximum growth rate and its corresponding unstable wave number. The theoretical behaviour predicted by the dispersion diagrams was compared with the experimental results obtained by the same authors in previous works from the atomization of alginate solution using an air-blast atomizer. It was found that the instability model proposed justify the experimental effects found for the atomization of the fluid and under the work range for alginate flow rate and viscosity and air flow rate.
© 2007 Elsevier B.V. All rights reserved.

Keywords: Polymer; Atomization; Air-blast atomizer; Instability; Growth rate

1. Introduction

The process of transforming bulk liquid into a large number of droplets and dispersing them in the form of a spray in a gaseous environment is called as atomization. Liquid atomization is of importance in numerous applications such as fuel injection in engines, crop spraying, food drying, manufacturing of pharmaceutical products, and lately microencapsulation applications [1].

During the last decade atomization techniques as air-blast or twin-fluid atomization has been widely used [2–4]. In air-blast atomization, low-speed liquid jets are accelerated by the surrounding high-speed gas flow, usually in the spray flow direction. The liquid is subjected to both tensile and shearing stresses. The magnitude of the extension has been shown to be significant for applications involving polymer solutions. Twin-fluid atomizers have a number of advantages over pressure atomizers including lower requirements for the liquid injection pressure and finer sprays. Unfortunately, the process of air-blast atomization is very complex and its physical mechanisms are not fully understood [1].

Theoretical and experimental studies on the mechanism of atomization have been carried out by Rayleigh, Tyler, Weber, Haenlein, Ohnesorge and Castleman [1]. Detailed reviews of earlier work have been published by Giffen and Muraszew [5], and more recently by Chigier [6], and Lefebvre [1] from these studies it can be concluded that the wave mechanism has been found the widest acceptance among the mechanisms of atomization. According to this theory the disintegration of liquid sheets or liquid jets is caused by the growth of unstable waves at the liquid–gas interface due to the aerodynamic interactions between the liquid and the gas. This type of instability is referred to as Kelvin–Helmholtz instability [7] and is characterized by unstable waves that appear in the fluid interface between two superimposed fluids of differing densities and velocities.

The waves are generated by factors such as pressure fluctuations or turbulence in the gas stream or liquid stream [8–9]. Due to aerodynamic interactions, the perturbations grow in magnitude and reach a maximum value. When the dynamic pressure ($\rho_a U_a^2/2$) of the air stream in air-blast atomization is large enough, the amplitude of the surface waves will grow if their wavelength (λ) exceeds a minimum value [8–11]. There exists a dominant or most unstable wave number corresponding to the maximum growth rate and when the amplitude of the disturbance reaches a critical value, the wave detaches from the sheet to form ligaments, which rapidly collapse, forming drops.

* Corresponding author.
E-mail address: emvalle@usal.es (E.M.M. Del Valle).

1385-8947/$ – see front matter © 2007 Elsevier B.V. All rights reserved.
doi:10.1016/j.cej.2007.01.028

Nomenclature

A	vortex strength (m^2/s)
D	injector exit diameter, diameter of liquid jet (μm)
D_a	inner diameter of liquid sheet (μm)
D_b	outer diameter of liquid sheet (μm)
$D_{0.9}$	diameter at the 90th percentile (μm)
$D_{0.1}$	diameter at the 10th percentile (μm)
$D_{0.5}$	diameter at the 50th percentile (μm)
g	gas-to-liquid density ratio
h	ratio of inner and outer radius
I_n	nth order modified Bessel function of first kind
k	axial wave number (m^{-1})
K_n	nth order modified Bessel function of second kind
n	Azimuthal wave number
p'	disturbance pressure (N/m^2)
P	mean pressure (N/m^2)
r	radial coordinate (m)
R_a	inner radius of liquid sheet (m)
R_b	outer radius of liquid sheet (m)
t	time (s)
u	disturbance axial velocity (m/s)
U	mean axial velocity (m/s)
v	disturbance radial velocity (m/s)
V	mean radial velocity (m/s)
w	disturbance tangential velocity (m/s)
W	mean tangential velocity (m/s)
We	Weber number ($We = \rho_l U^2 D_b/\sigma$)
Z	Ohnesorge number, $\mu/(\rho_l \sigma D_b)^{1/2}$

Greek letters

η	displacement disturbance (m)
μ	fluid viscosity (Ns/m^2)
ρ	fluid density (kg/m^3)
σ	surface tension (kg/s^2)
ω	temporal frequency (s^{-1})
Ω	angular velocity (s^{-1})
θ	Azimuthal angle (radian)
ϕ	phase difference (radian)

Subscripts

i	inner gas
l	liquid phase
o	outer air
s	based on swirling component

Herrero et al. [12], based on atomization processes, have developed a new technology of production of microcapsules based on a non-Newtonian fluid alginate solutions, which produced microcapsules ranged between 1 and 50 μm, with control size and a particle size distribution with a relative span factor, $(D_{0.9} - D_{0.1})/D_{0.5}$, less than 1.4. They have studied the effect of the alginate solution viscosity and flow rate and air flow rate. They have also developed a mathematical semi-empirical model, based on the wave mechanism, to predict the size of the microcapsules produced by atomization [13].

Therefore, the main aim of this work is to develop a temporal stability analysis to model the atomization of a swirling viscous annular liquid sheet emanating from an air-blast atomizer subject to inner and outer inviscid swirling air streams. The dimensionless dispersion equation that governs the instability of a viscous annular liquid sheet under swirling air streams will be derived. Usually this equation is derived and solved for an inviscid liquid sheet, because this analysis should be used to improve the fuel atomization in aircraft engines. The elimination of the liquid viscosity in the main equations does not affect very much the solution in this case. In microencapsulation application, where polymers are used the viscosity cannot be eliminated because is a very important parameter especially when the polymer has a non-Newtonian behaviour. However, in this work low polymer concentrations have been used, therefore it would be possible to consider the fluid as a Newtonian liquid [14]. For that reason, numerical solutions to the dispersion equation under a wide range of liquid viscosity values, and flow conditions will be carried out to investigate the effects of the liquid and gas on the maximum growth rate and its corresponding unstable wave number. So, the theoretical behaviour predicted by the dispersion diagrams will be compared with the experimental results obtained previously from the atomization of alginate solution, using an air-blast atomizer.

2. Linear stability analysis

2.1. Model assumptions

The stability model considers a swirling viscous annular liquid sheet subject swirling airstreams as shown in Fig. 1. Gas phases are assumed to be inviscid and incompressible. The basic

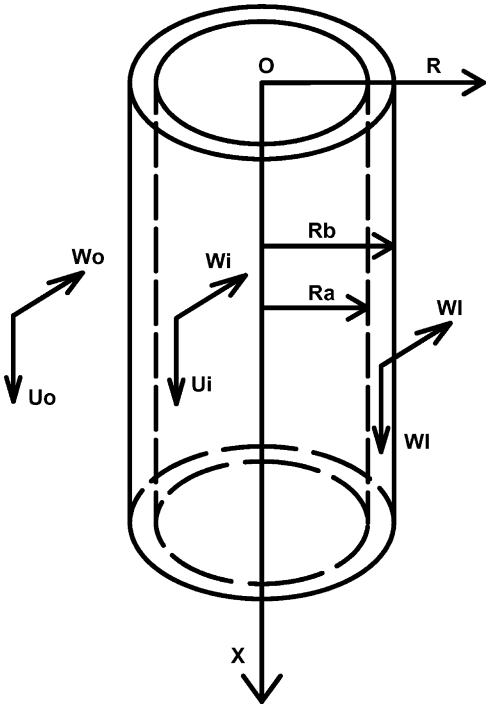

Fig. 1. Annular swirling viscous liquid sheet subject to swirling airstreams.

flow velocities for liquid, inner gas and outer gas are assumed to be $(U_l, 0, A_l/r)$, $(U_i, 0, \Omega r)$, $(U_o, 0, A_o/r)$, respectively. Inner gas swirl profile is assumed to be solid body rotation and outer gas swirl profile is of free vortex type. The assumed velocity profiles are similar to the profiles in an air blast atomizer [15].

Sheet instability occurs due to the growth of unstable waves at the liquid–gas interface. The growth rates of these unstable waves are governed by fluid properties, nozzle geometry and competition of forces acting on the interface including viscous, pressure, inertial, surface tension, and centrifugal force. There exists a dominant or most unstable wave number corresponding to the maximum growth rate. A temporal linear instability analysis is conducted to determine the maximum growth rate and the most unstable wave number.

2.2. Linearized disturbance equations

The governing equations for viscous annular fluid flows are the continuity and Navier–Stokes equations that in cylindrical coordinate system are:

Continuity:

$$\frac{V}{r} + \frac{\partial V}{\partial r} + \frac{1}{r}\frac{\partial W}{\partial \theta} + \frac{\partial U}{\partial x} = 0 \tag{1}$$

Momentum:

$$\frac{\partial U}{\partial t} + V\frac{\partial U}{\partial r} + \frac{W}{r}\frac{\partial U}{\partial \theta} + U\frac{\partial U}{\partial x} = -\frac{1}{\rho}\frac{\partial p}{\partial x} + \nu\left(\frac{\partial^2 U}{\partial r^2} + \frac{1}{r}\frac{\partial U}{\partial r} + \frac{1}{r^2}\frac{\partial^2 U}{\partial \theta^2} + \frac{\partial^2 U}{\partial x^2}\right) \tag{2}$$

$$\frac{\partial V}{\partial t} + V\frac{\partial V}{\partial r} + \frac{W}{r}\frac{\partial V}{\partial \theta} + U\frac{\partial V}{\partial x} - \frac{W^2}{r} = -\frac{1}{\rho}\frac{\partial p}{\partial r} + \nu\left(\frac{\partial^2 V}{\partial r^2} + \frac{1}{r}\frac{\partial V}{\partial r} + \frac{1}{r^2}\frac{\partial^2 V}{\partial \theta^2} - \frac{V}{r^2} + \frac{2}{r^2}\frac{\partial W}{\partial \theta} + \frac{\partial^2 V}{\partial x^2}\right) \tag{3}$$

$$\frac{\partial W}{\partial t} + V\frac{\partial W}{\partial r} + \frac{W}{r}\frac{\partial W}{\partial \theta} + U\frac{\partial W}{\partial x} + \frac{VW}{r} = -\frac{1}{\rho}\frac{\partial p}{\partial \theta} + \nu\left(\frac{\partial^2 W}{\partial r^2} + \frac{1}{r}\frac{\partial W}{\partial r} + \frac{1}{r^2}\frac{\partial^2 W}{\partial \theta^2} - \frac{W}{r^2} + \frac{2}{r^2}\frac{\partial V}{\partial \theta} + \frac{\partial^2 W}{\partial x^2}\right) \tag{4}$$

In order to obtain the linearized disturbance equations, let

$$U = \bar{U} + u, \qquad V = v, \qquad W = \bar{W} + w, \qquad p = \bar{P} + p' \tag{5}$$

where the overbar represents the mean flow quantities and u, v, w and p' indicates disturbances. The disturbances are assumed to be of the form:

$$(u, v, w, p') = (\hat{u}(r), \hat{v}(r), \hat{w}(r), \hat{p}(r))\, e^{i(kx+n\theta-\omega t)} \tag{6}$$

where $\wedge$ indicates the disturbance amplitude which is a function for r only. For the temporal analysis, the wave number k and n are real while frequency ω is complex. The maximum value of imaginary ω represents the maximum growth rate of the disturbance, and the corresponding value of k represents the most unstable wave number.

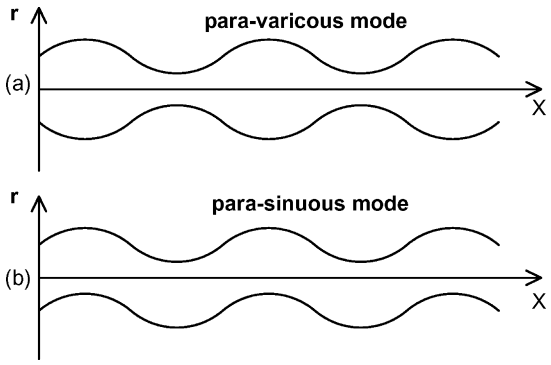

Fig. 2. A schematic description of (a) the para-varicous mode and (b) the para-sinuous mode.

For such an annular jet, unstable waves develop on both the inner and outer surfaces, which may be in phase or out of phase. When the waves develop in phase, the shapes of the waves are antisymmetric with respect to the mid-plane of liquid sheet, and this kind of instability mode is called the para-sinuous mode (Fig. 2a). When the waves develop out of phase, the waves are symmetric with respect to the mid-plane of the liquid sheet, and this mode is called the para-varicous mode (Fig. 2b) [16].

The displacement disturbances at the inner and outer interfaces are given by the following equations:

$$\eta_i(x, \theta, t) = \eta_i\, e^{i(kx+n\theta-\omega t)+i\phi} \tag{7}$$

$$\eta_o(x, \theta, t) = \eta_o\, e^{i(kx+n\theta-\omega t)} \tag{8}$$

Here ϕ indicates the phase difference between the displacement at the inner and the outer interface.

Substituting Eq. (5) into Eqs. (1)–(4), subtracting the mean flow equations and neglecting the second-order terms, it is achieved the linearized equations for velocity and pressure disturbances.

In order to determine the effect of the various forces, properties of fluids and other geometric parameters, the linearized equations are non-dimensionlized by introducing the following dimensionless parameters:

$$We_l = \frac{\rho_l U_l^2 D_b}{\sigma}, \qquad We_i = \frac{\rho_i U_i^2 D_b}{\sigma}, \qquad We_o = \frac{\rho_o U_o^2 D_b}{\sigma},$$

$$We_s = \frac{\rho_l W_l^2 D_b}{\sigma}, \qquad We_{si} = \frac{\rho_i W_i^2 D_b}{\sigma}, \qquad We_{so} = \frac{\rho_o W_o^2 D_b}{\sigma},$$

$$Z = \frac{\mu_l}{(\rho_l \sigma D_b)^{1/2}}, \qquad g_i = \frac{\rho_i}{\rho_l}, \qquad g_o = \frac{\rho_o}{\rho_l}, \qquad \bar{k} = kR_b,$$

$$\bar{\omega} = \frac{\omega R_b}{U_l}, \qquad \frac{U_i}{U_l} = \sqrt{\frac{We_i}{We_l}\frac{1}{g_i}}, \qquad \frac{U_o}{U_l} = \sqrt{\frac{We_o}{We_l}\frac{1}{g_o}},$$

$$\frac{A_l}{U_l R_b} = \sqrt{\frac{We_s}{We_l}}, \qquad \frac{A_o}{U_l R_b} = \sqrt{\frac{We_{so}}{We_l}\frac{1}{g_o}},$$

$$\frac{\Omega R_b}{U_l} = \sqrt{\frac{We_{si}}{We_l}\frac{1}{g_i}}, \qquad \bar{s} = (\overline{k^2} + Z(-i\bar{\omega} + i\bar{k}))^{1/2},$$

$$h = \frac{R_a}{R_b}$$

As dimensionless parameters it has included the Weber number, which represents the ratio of aerodynamic force to surface tension, and the Ohnesorge number, which contains only the properties of the globules formed in primary atomization before they split up into smaller drops during secondary atomization. Ohnesorge number is sometimes called a stability group because it provides an indication of the resistance of a globule to further disintegration, but it is also called a viscosity group because it accounts for the effect of liquid viscosity on the globule. Ohnesorge number is used in momentum transfer in general and atomization calculations in particular.

Since it is considered three-dimensional perturbations, the two surface waves may also be axi-symmetric ($n=0$) or non-axi-symmetric ($n=1$) with respect to the central axis of the jet. Several studies have examined the disintegration of non-swirling liquid sheets and liquid jets subject to axi-symmetric disturbances. Li and Tankin [17] conducted a temporal instability analysis of a thin viscous liquid sheet in an inviscid gas medium and found axi-symmetrical disturbances to control the instability process for small Weber numbers. Liao et al. [18] reported axi-symmetric mode to be the dominant mode in the absence of air swirl velocity. Chen et al. [19] carried out a linear stability analysis for an annular viscous jet subject to three-dimensional disturbances and showed axi-symmetric mode to be the most unstable mode in the system. As such we have restricted the present analysis to the axi-symmetric mode. Perturbation in the Azimuthal direction is taken as zero, i.e. $\hat{w} = 0$.

After applying these restrictions it is obtained the linearized disturbance equations for the liquid phase and the gas phase.

The disturbance equations for the liquid phase are

$$\hat{u}(i\bar{k}) + \frac{d\hat{v}}{dr} + \frac{v}{r} = 0 \tag{9}$$

$$\hat{u}(-i\bar{\omega} + i\bar{k}) = -i\bar{k}\hat{p} + Z\left(\frac{d^2\hat{u}}{dr^2} + \frac{1}{r}\frac{d\hat{u}}{dr} - \frac{\hat{u}}{r^2}(\overline{k^2}r^2)\right) \tag{10}$$

$$\hat{v}(-i\bar{\omega} + i\bar{k}) = -\frac{d\hat{p}}{dr} + Z\left(\frac{d^2\hat{v}}{dr^2} + \frac{1}{r}\frac{d\hat{v}}{dr} - \frac{\hat{v}}{r^2}(\overline{k^2}r^2 + 1)\right) \tag{11}$$

The disturbance equations for the gas phase are

Inner gas:

$$\hat{u}(i\bar{k}) + \frac{d\hat{v}}{dr} + \frac{v}{r} = 0 \tag{12}$$

$$\hat{u}\left(-i\bar{\omega} + i\bar{k}\sqrt{\frac{We_i}{We_l}\frac{1}{g_i}}\right) = -\frac{1}{g_i}i\bar{k}\hat{p} \tag{13}$$

$$\hat{v}\left(-i\bar{\omega} + i\bar{k}\sqrt{\frac{We_i}{We_l}\frac{1}{g_i}}\right) = -\frac{1}{g_i}\frac{d\hat{p}}{dr} \tag{14}$$

Outer gas:

$$\hat{u}(i\bar{k}) + \frac{d\hat{v}}{dr} + \frac{v}{r} = 0 \tag{15}$$

$$\hat{u}\left(-i\bar{\omega} + i\bar{k}\sqrt{\frac{We_o}{We_l}\frac{1}{g_o}}\right) = -\frac{1}{g_o}i\bar{k}\hat{p} \tag{16}$$

$$\hat{v}\left(-i\bar{\omega} + i\bar{k}\sqrt{\frac{We_o}{We_o}\frac{1}{g_i}}\right) = -\frac{1}{g_o}\frac{d\hat{p}}{dr} \tag{17}$$

2.3. Boundary conditions

In the same way, under the above conditions, the following dimensionless boundary conditions are necessary to solve the linearized disturbance equations. The first boundary condition is the kinematic condition that a particle of fluid on the surface moves with the surface so as to remain on the surface or in other words, the velocity components normal to the interface is continuous across the interface:

Liquid:

$$v_l = \frac{\partial\eta_i}{\partial t} + \frac{\partial\eta_i}{\partial x} \quad \text{at } r = h \tag{18}$$

$$v_l = \frac{\partial\eta_o}{\partial t} + \frac{\partial\eta_o}{\partial x} \quad \text{at } r = 1 \tag{19}$$

Inner gas:

$$v_i = \frac{\partial\eta_i}{\partial t} + \frac{\partial\eta_i}{\partial x}\sqrt{\frac{We_i}{We_l}\frac{1}{g_i}} \quad \text{at } r = h \tag{20}$$

Outer gas:

$$v_o = \frac{\partial\eta_o}{\partial t} + \frac{\partial\eta_o}{\partial x}\sqrt{\frac{We_o}{We_l}\frac{1}{g_o}} \quad \text{at } r = 1 \tag{21}$$

Due to the inviscid assumption for the gas streams in the axial and Azimuthal directions, viscous stress at the liquid–gas interface is zero. This is expressed as

$$\frac{\partial u}{\partial r} + \frac{\partial v}{\partial x} = 0 \quad \text{at } r = h, 1 \tag{22}$$

The last boundary condition considers the balance between the surface stresses on both sides of the liquid–gas interface,

including the pressure jump across the interface due to surface tension and viscous forces. This boundary condition is known as the dynamic boundary condition and is given by

$$p_l' - p_i' = \frac{1}{h^2 We_l}\left(\eta_i + h^2\frac{\partial^2\eta_i}{\partial x^2}\right) + h\frac{We_{si}}{We_l}\eta_i - \frac{We_s}{We_l}\frac{\eta_i}{h^3} + 2Z\frac{\partial v}{\partial r} \quad \text{at } r = h \tag{23}$$

$$p_l' - p_o' = -\frac{1}{We_l}\left(\eta_o + \frac{\partial^2\eta_o}{\partial x^2}\right) + \frac{We_{so}}{We_l}\eta_o - \frac{We_s}{We_l}\eta_o + 2Z\frac{\partial v}{\partial r} \quad \text{at } r = 1 \tag{24}$$

2.4. Pressure disturbance inside the liquid sheet

As the governing equations (Eqs. (9)–(11)) are linear, the solution is decompose into inviscid and viscous parts as

$$\hat{u} = \hat{u}_1 + \hat{u}_2 \tag{25}$$

$$\hat{v} = \hat{v}_1 + \hat{v}_2 \tag{26}$$

Here the subscripts 1 and 2 represent the inviscid and the viscous parts of the velocity perturbations, respectively [20]:

$$\hat{u}_1(i\bar{k}) + \frac{d\hat{v}_1}{dr} + \frac{\hat{v}_1}{r} = 0 \tag{27}$$

$$\hat{u}_1(-i\bar{\omega} + i\bar{k}) = -i\bar{k}\hat{p} \tag{28}$$

$$\hat{v}_1(-i\bar{\omega} + i\bar{k}) = -\frac{d\hat{p}}{dr} \tag{29}$$

$$\hat{u}_2(i\bar{k}) + \frac{d\hat{v}_2}{dr} + \frac{\hat{v}_2}{r} = 0 \tag{30}$$

$$\hat{u}_2(-i\bar{\omega} + i\bar{k}) = Z\left(\frac{d^2\hat{u}_2}{dr^2} + \frac{1}{r}\frac{d\hat{u}_2}{dr} - \frac{\hat{u}_2}{r^2}(\overline{k^2}r^2)\right) \tag{31}$$

$$\hat{v}_2(-i\bar{\omega} + i\bar{k}) = Z\left(\frac{d^2\hat{v}_2}{dr^2} + \frac{1}{r}\frac{d\hat{v}_2}{dr} - \frac{\hat{v}_2}{r^2}(\overline{k^2}r^2 + 1)\right) \tag{32}$$

Differentiating Eq. (28) with respect to r and eliminating $\hat{p}$ from Eqs. (28) and (29):

$$\hat{v}_1 = -\frac{1}{i\bar{k}}\frac{d\hat{u}_1}{dr} \tag{33}$$

Substituting Eq. (33) in Eq. (27):

$$\left(\frac{d^2\hat{u}_1}{dr^2} + \frac{1}{r}\frac{d\hat{u}_1}{dr} - \frac{\hat{u}_1}{r^2}(\overline{k^2}r^2)\right) = 0 \tag{34}$$

The above equation is a Bessel equation which has a solution of the form:

$$\hat{u}_1 = C_1 I_0(\bar{k}r) + C_2 K_0(\bar{k}r) \tag{35}$$

Substituting Eq. (35) in Eqs. (33) and (28):

$$\hat{v}_1 = -iC_1 I_1(\bar{k}r) + iC_2 K_1(\bar{k}r) \tag{36}$$

$$\hat{p} = \frac{\bar{\omega} - \bar{k}}{\bar{k}}(C_1 I_0(\bar{k}r) + C_2 K_0(\bar{k}r)) \tag{37}$$

Let

$$\bar{s}^2 = (\overline{k^2} + Z(-i\bar{\omega} + i\bar{k})) \tag{38}$$

Rearranging Eqs. (31) and (32) and using Eq. (38), it is obtained the Bessel equations for $\hat{u}_2$ and $\hat{v}_2$:

$$\left(\frac{d^2\hat{u}_2}{dr^2} + \frac{1}{r}\frac{d\hat{u}_2}{dr} - \frac{\hat{u}_2}{r^2}(\overline{s^2}r^2)\right) = 0 \tag{39}$$

$$\left(\frac{d^2\hat{v}_2}{dr^2} + \frac{1}{r}\frac{d\hat{v}_2}{dr} - \frac{\hat{v}_2}{r^2}(\overline{s^2}r^2 + 1)\right) = 0 \tag{40}$$

The solutions for Eqs. (39) and (40) can be expressed in the following form:

$$\hat{u}_2 = M_1 I_0(\bar{s}r) + M_2 K_0(\bar{s}r) \tag{41}$$

$$\hat{v}_2 = M_3 I_1(\bar{s}r) + M_4 K_1(\bar{s}r) \tag{42}$$

Then, using Eqs. (25) and (26), the total velocity components are expressed as

$$\hat{u} = C_1 I_0(\bar{k}r) + C_2 K_0(\bar{k}r) + M_1 I_0(\bar{s}r) + M_2 K_0(\bar{s}r) \tag{43}$$

$$\hat{v} = -iC_1 I_1(\bar{k}r) + iC_2 K_1(\bar{k}r) + M_3 I_1(\bar{s}r) + M_4 K_1(\bar{s}r) \tag{44}$$

Using the boundary conditions (Eqs. (18), (19) and (22)) and utilizing the solutions from the Bessel equations, the constants C_1, C_2, M_1 to M_4 are determined:

$$C_1 = \frac{i(-i\bar{\omega} + i\bar{k})}{l_{18} I_1(\bar{k}h)}(\hat{\eta}_i e^{i\phi} l_{16} - \hat{\eta}_o l_{17}) \tag{45}$$

$$C_2 = \frac{2\bar{k}^2(-i\bar{\omega} + i\bar{k})}{l_{13}}(\hat{\eta}_i e^{i\phi} I_1(\bar{k}) l_{14} - \hat{\eta}_o l_{15}) \tag{46}$$

$$M_1 = \frac{2\bar{k}\bar{s}\, i(-i\bar{\omega} + i\bar{k})}{l_9 l_{11}}(\hat{\eta}_i e^{i\phi} I_1(\bar{k}) l_{12} - \hat{\eta}_o l_9 l_{10}) \tag{47}$$

$$M_2 = \frac{2\bar{k}\bar{s}\, i(-i\bar{\omega} + i\bar{k})}{l_{11}}(\hat{\eta}_i e^{i\phi} I_1(\bar{k}) l_4 l_6 - \hat{\eta}_o l_9) \tag{48}$$

$$M_3 = \frac{2\bar{k}^2(-i\bar{\omega} + i\bar{k})}{l_9 l_{11}}(\hat{\eta}_i e^{i\phi} I_1(\bar{k}) l_{12} - \hat{\eta}_o l_9 l_{10}) \tag{49}$$

$$M_4 = -\frac{2\bar{k}^2(-i\bar{\omega} + i\bar{k})}{l_{11}}(\hat{\eta}_i e^{i\phi} I_1(\bar{k}) l_4 l_6 - \hat{\eta}_o l_9) \tag{50}$$

The coefficients of the constants are available in Appendix A.

Then, the pressure disturbance inside the liquid sheet (Eq. (37)):

$$p_l' = \frac{\bar{\omega} - \bar{k}}{\bar{k}}\left(\frac{2\bar{k}^2(-i\bar{\omega} + i\bar{k})}{l_{13}}(\hat{\eta}_i e^{i\phi} I_1(\bar{k}) l_{14} - \hat{\eta}_o l_{15}) I_0(\bar{k}r) + \frac{2\bar{k}^2(-i\bar{\omega} + i\bar{k})}{l_{13}}(\hat{\eta}_i e^{i\phi} I_1(\bar{k}) l_{14} - \hat{\eta}_o l_{15}) K_0(\bar{k}r)\right) e^{i(\bar{k}x - \bar{\omega}t)} \tag{51}$$

2.5. Pressure disturbance in inner gas

In the same way that in Section 2.4, from Eqs. (12)–(14) and (20), and considering that for inner gas, as $r \to 0$, $K_0(\bar{k}r) \to \infty$ (which is due to the fact that amplitude of the velocity disturbance is bounded at the centreline of the sheet), it is obtained the pressure disturbance in inner gas:

$$p_i' = \left(\frac{g_i(\bar{\omega} - \bar{k}\sqrt{(We_i/We_l)(1/g_i)})^2 \hat{\eta}_i \, e^{i\phi}}{\bar{k} I_1(\bar{k}h)} I_0(\bar{k}h) \right) e^{i(\bar{k}x - \bar{\omega}t)} \tag{52}$$

2.6. Pressure disturbance in outer gas

In the same way that in Section 2.4, from the Eqs. (15)–(17) and (21), and considering that for outer gas, as $r \to \infty$, $I_0(\bar{k}r) \to \infty$ (which is due to the fact that amplitude of the velocity disturbance is bounded at infinity), it is obtained the pressure disturbance in outer gas:

$$p_o' = \left(-\frac{g_o(\bar{\omega} - \bar{k}\sqrt{(We_o/We_l)(1/g_o)})^2 \hat{\eta}_o}{\bar{k} K_1(\bar{k})} K_0(\bar{k}) \right) e^{i(\bar{k}x - \bar{\omega}t)} \tag{53}$$

2.7. Non-dimensional dispersion equation

The final dimensionless dispersion equation is obtained by substitution of Eqs. (52) and (53) into Eqs. (23) and (24), respectively. These lead to the following expressions:

$$\alpha(E_1 + E_2 + E_3) + (E_4 + E_5) = 0 \tag{54}$$

$$\alpha(F_1 + F_2 + F_3) + (F_4 + F_5) = 0 \tag{55}$$

where $\alpha = (\hat{\eta}_i/\hat{\eta}_o)\, e^{i\phi}$

Eliminating α from the above two equations, it is achieved a fourth-order non-dimensional dispersion equation of the form:

$$GH_1 - G_1 H = 0 \tag{56}$$

Details of the expressions in Eqs. (54)–(56) are available in Appendix A. In other words, the non-dimensional dispersion equation can be simply stated as

$$f(\bar{\omega}, \bar{k}, \bar{s}, g_i, g_o, Z, We_l, We_i, We_o, We_s, We_{si}, We_{so}, h) = 0 \tag{57}$$

Unlike the inviscid case, the final dispersion equation does not have a closed form solution and is solved numerically using *Mathematica*™. The Secant method is used where two starting complex guess values are required to determine the roots of the dimensionless dispersion equation. Results from the inviscid case are taken as starting guess values. By varying the value of k, it is solved for the root with the maximum imaginary part that represents the maximum growth rate of disturbance corresponding to the most unstable wave number.

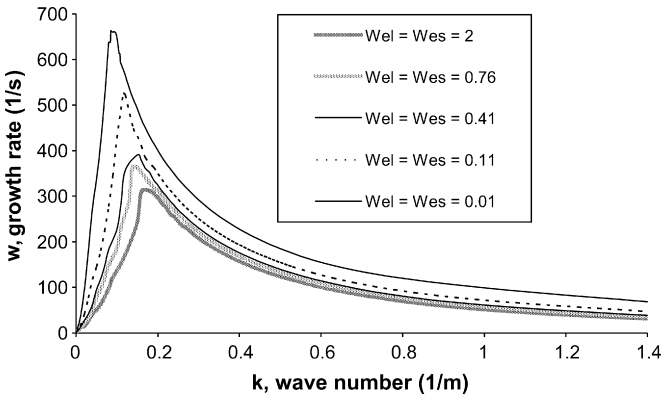

Fig. 3. Dispersion diagram at $We_i = We_o = We_{si} = We_{so} = 35{,}128$; $Z = 0.2$; $We_l = We_s = 0.01 - 2$.

3. Results and discussion

In the process of determining the disintegration of the swirling viscous annular liquid sheet emanating from an air-blast prefilmer, the final non-linear dimensionless dispersion equation was derived based on the assumption that the inner and outer gas flows are invisid moving axially outward with swirling velocity components. A complete parametric study has been conducted to insolate the effect of flow conditions and viscosity on the instability of the liquid sheet. The non-dimensional parameters utilized in the final dispersion equation are the axial Weber numbers, We_l, We_i, and We_o, swirling Weber numbers, We_s, We_{si}, and We_{so}, Ohnesorge number, Z, axial wave number k, gas to liquid air density ratio, g_i and g_o, and the annular liquid sheet inner and outer radii ratio, h.

The frequency with the maximum imagery part represents the most unstable wave that is the perturbation that grows more rapidly than any other and for that reason it dominates the liquid sheet breakup process. Therefore, the most unstable wave number is related to the mean drop size. The growth rate can be related to the breakup length of the liquid sheet. Higher growth rate indicates shorter breakup length. As such the most unstable wave number and the maximum growth rate are two important parameters that will determine the resulting spray characteristics. These parameters are obtained for a number of flow geometry conditions and are discussed below. The results are presented in three graphs (Figs. 3–5) $\omega = f(k)$ called dispersion diagrams. These figures show the expected bell shape, commonly encountered in linear theory analysis. In each situation, a finite range of unstable perturbations, i.e. showing a positive growth rate, was obtained.

3.1. Liquid flow rate variation

The influence of the liquid flow rate variation in the growth rate is shown in Fig. 3. These results were obtained for an atomization nozzle of 1.8 mm in previous works conducted by the authors [12]. The experimental conditions were the following: a constant value of pressurized flow air of 138,000 L/min ($We_i = We_o = We_{si} = We_{so} = 35{,}128$) and the liquid flow rate was modified ranged from 0.003 L/min to 0.037 L/min

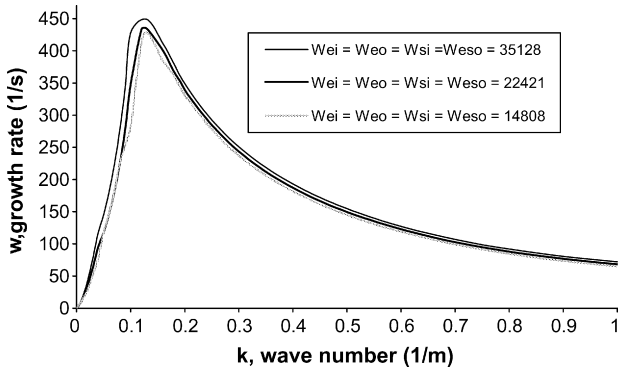

Fig. 4. Dispersion diagram at $We_l = We_s = 0.11$; $Z = 0.2$; $We_i = We_o = We_{si} = We_{so} = 14{,}808 - 35{,}128$.

($We_l = We_s = 0.01$ to $We_l = We_s = 2$). The liquid viscosity was maintained constant at 64.5 mPa s ($Z = 0.2$). It can be seen in Fig. 3 that when the liquid flow decrease, the growth rate increase, which indicates shorter breakup length and smaller drops.

These results are in a very good agreement with the experimental work of Herrero et al. [12], where it was found experimentally that the particle size decreases when it is decreased the liquid flow. To justify this effect it should be taking into account that lower values of liquid flow rate result in thinner films. It was observed that thinner liquid films break down into smaller drops.

3.2. Air flow rate variation

The influence of the air flow rate variation in the growth rate is shown in Fig. 4. These results were obtained for an atomization nozzle of 1.8 mm in previous works conducted by the authors [12]. The experimental conditions were the following: a constant value of liquid flow of 0.009 L/min ($We_l = We_s = 0.11$) and the air flow rate was modified ranged from 89,600 L/min to 138,000 L/min ($We_i = We_o = We_{si} = We_{so} = 14{,}808$ to $We_i = We_o = We_{si} = We_{so} = 35{,}128$). The liquid viscosity was maintained constant at 64.5 mPa s ($Z = 0.2$). It can be seen in Fig. 4 that when the air flow increase, the growth rate increase, which indicates shorter breakup length and smaller drops.

These results are in a very good agreement with the experimental work of Herrero et al. [12], where it was found experimentally that the particle size decreases when it is increase the air flow. To justify this effect it should be take into account that the liquid/air interaction produces waves that become unstable and disintegrate into fragments. These fragments then, contract into ligaments, which in turn break down into drops. It has been proved that when the air velocity is increased, the liquid sheet disintegrates earlier and ligaments are formed nearer the lip. These ligaments tend to be thinner and shorter and disintegrate into smaller drops. For a constant liquid sheet thickness the breakup length decreases with increase in the relative velocity between the air and the liquid.

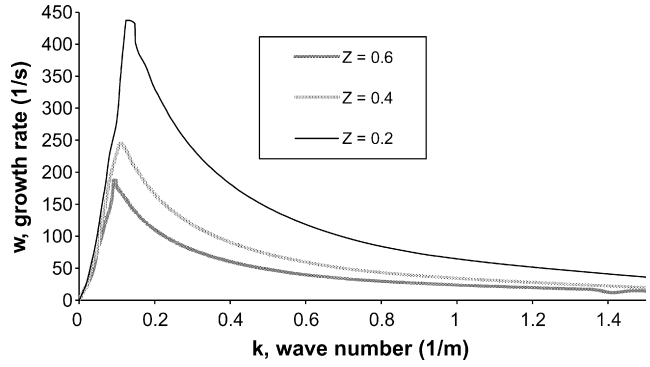

Fig. 5. Dispersion diagram at $We_i = We_o = We_{si} = We_{so} = 14{,}808$; $We_l = We_s = 0.11$; $Z = 0.2 - 0.6$.

3.3. Liquid viscosity effect

The influence of the liquid viscosity in the growth rate is shown in Fig. 5. These results were obtained for an atomization nozzle of 1.8 mm in previous works conducted by the authors [12]. The experimental conditions were the following: a constant value of pressurized flow air of 89,600 L/min ($We_i = We_o = We_{si} = We_{so} = 14{,}808$), a constant value of liquid flow of 0.009 L/min ($We_l = We_s = 0.11$) and the liquid viscosity was modified ranged from 64.5 mPa s to 190.0 mPa s ($Z = 0.2$–0.6).

It can be seen in Fig. 5 that when the liquid viscosity decrease, the growth rate increase, which indicates shorter breakup length and smaller drops.

These results are in a very good agreement with the experimental work of Herrero et al. [12], where it was found that the particle size increases when it was increased the liquid viscosity. It can be explained if we consider that the liquid viscosity of the fluid to be atomize, tends to avoid the growth of the instabilities that cause the rupture of the jet or liquid sheet, delaying, therefore, the disintegration of the liquid and increasing the size of the microcapsules. In addition, lower values of liquid viscosity result in thinner films that break down into smaller drops.

4. Conclusions

A temporal instability study of a swirling annular liquid sheet of polymer produced by air-blast atomization has been done in order to model an atomization process to generate microcapsules. The dimensionless dispersion equation that governs the instability of a viscous annular liquid sheet under swirling air streams is derived. Numerical solutions to the dispersion equation under a wide range of flow conditions are carried out to investigate the effects of the liquid and gas flow on the maximum growth rate. The growth rate can be related to the breakup length of the liquid sheet.

It has been observed that when the polymer flow decrease, the growth rate increase, which indicates shorter breakup length and smaller drops because of lower values of liquid flow rate result in thinner films that break down into smaller drops.

An analysis of the dispersion diagrams shows that when the air flow increase, the growth rate increase, which indicates shorter breakup length and smaller drops, because of the liquid/air interaction produces waves that become unstable and disintegrate into fragments, and contract into ligaments, which in turn break down into drops.

When the polymer viscosity decrease, the growth rate increases, this indicates shorter breakup length and smaller drops.

The theoretical behaviour predicted by the dispersion diagrams were compared with the experimental results obtained from the atomization of alginate solution using an air-blast atomizer. It was found that the instability model proposed justify the experimental effects found for the atomization of a fluid and under the work range for alginate flow rate and viscosity and air flow rate.

Acknowledgment

The authors gratefully acknowledge Prof. Dr. D. Jose Angel Dominguez from the Mathematics Department of the University of Salamanca for the help with Mathematica. This research was supported by funds from the Ministry of Science and Education (MEC). The authors gratefully acknowledge the financial support.

Appendix A. Coefficients of the constants

The expressions for the coefficients used in determining the constants (Eqs. (45)–(50)) are

$$l_1 = 2\bar{k}^2 \mathrm{i} I_1(\bar{k}) K_1(\bar{k}h) - 2\bar{k}^2 \mathrm{i} K_1(\bar{k}) I_1(\bar{k}h) \tag{A.1}$$

$$l_2 = 2\bar{k}^2 I_1(\bar{k}) I_1(\bar{s}h) - (\bar{s}^2 + \bar{k}^2) I_1(\bar{s}) I_1(\bar{k}h) \tag{A.2}$$

$$l_3 = 2\bar{k}^2 I_1(\bar{k}) K_1(\bar{s}h) - (\bar{s}^2 + \bar{k}^2) K_1(\bar{s}) I_1(\bar{k}h) \tag{A.3}$$

$$l_4 = (\bar{k}^2 - \bar{s}^2) I_1(\bar{s}) \tag{A.4}$$

$$l_5 = (\bar{k}^2 - \bar{s}^2) K_1(\bar{s}) \tag{A.5}$$

$$l_6 = 2\bar{k}^2 K_1(\bar{k}) I_1(\bar{k}h) - 2\bar{k}^2 \mathrm{i} K_1(\bar{k}h) I_1(\bar{k}) \tag{A.6}$$

$$l_7 = (\bar{s}^2 + \bar{k}^2) I_1(\bar{s}) I_1(\bar{k}h) - (\bar{s}^2 + \bar{k}^2) I_1(\bar{s}h) I_1(\bar{k}) \tag{A.7}$$

$$l_8 = (\bar{s}^2 + \bar{k}^2) K_1(\bar{s}) I_1(\bar{k}h) - (\bar{s}^2 + \bar{k}^2) K_1(\bar{s}h) I_1(\bar{k}) \tag{A.8}$$

$$l_9 = l_2 l_6 - l_1 l_7 \tag{A.9}$$

$$l_{10} = l_3 l_6 - l_1 l_8 \tag{A.10}$$

$$l_{11} = l_5 l_9 - l_{10} l_4 \tag{A.11}$$

$$l_{12} = l_6 l_{11} - l_6 l_4 l_{10} \tag{A.12}$$

$$l_{13} = l_6 l_9 l_{11} \tag{A.13}$$

$$l_{14} = l_8 l_9 l_6 l_4 - l_7 l_{12} \tag{A.14}$$

$$l_{15} = l_8 l_9 l_9 - l_7 l_9 l_{10} \tag{A.15}$$

$$l_{16} = l_{13} l_9 l_{11} - 2\bar{k}^2 \mathrm{i} K_1(\bar{k}h) I_1(\bar{k}) l_9 l_{11} l_{14} - 2\bar{k}^2 I_1(\bar{k}) I_1(\bar{s}h) l_{12} l_{13} + 2\bar{k}^2 I_1(\bar{k}) K_1(\bar{s}h) l_9 l_{13} l_6 l_4 \tag{A.16}$$

$$l_{17} = 2\bar{k}^2 K_1(\bar{s}h) l_{13} l_9 l_9 - 2\bar{k}^2 \mathrm{i} K_1(\bar{k}h) l_9 l_{11} l_{15} - 2\bar{k}^2 I_1(\bar{s}h) l_9 l_{13} l_{10} \tag{A.17}$$

$$l_{18} = l_{13} l_9 l_{11} \tag{A.18}$$

The expressions involved in Eqs. (54)–(56) are

$$E_1 = -\frac{(-\mathrm{i}\bar{\omega} + \mathrm{i}\bar{k})^2}{\bar{k} l_{18} I_1(\bar{k}h)} I_o(\bar{k}h) l_{16} + \frac{2\mathrm{i}\bar{k}^2 (-\mathrm{i}\bar{\omega} + \mathrm{i}\bar{k})^2}{l_{13}\bar{k}} K_o(\bar{k}h) I_1(\bar{k}) l_{14} - \frac{(-\bar{\omega} + \bar{k}\sqrt{(We_i/We_l)(1/g_i)})^2 g_i I_o(\bar{k}h)}{\bar{k} I_o'(\bar{k}h)} - \frac{2Z(-\mathrm{i}\bar{\omega} + \mathrm{i}\bar{k}) I_1'(\bar{k}h)(\bar{k}) l_{16}}{l_{18} I_1(\bar{k}h)} \tag{A.19}$$

$$E_2 = -\frac{4Z\mathrm{i}(\bar{k})^3 (-\mathrm{i}\bar{\omega} + \mathrm{i}\bar{k}) K_1'(\bar{k}h)}{l_{13}} I_1(\bar{k}) l_{14} - \frac{4Z\bar{k}^2 (-\mathrm{i}\bar{\omega} + \mathrm{i}\bar{k})\bar{s} I_1'(\bar{s}h) I_1(\bar{k}) l_{12}}{l_9 l_{11}} + \frac{4Z\bar{k}^2 (-\mathrm{i}\bar{\omega} + \mathrm{i}\bar{k})\bar{s} K_1'(\bar{s}h)}{l_{11}} l_6 l_4 I_1(\bar{k}) \tag{A.20}$$

$$E_3 = -\frac{1}{h^2 We_l}(1 - h^2\bar{k}^2) - h\frac{We_{si}}{We_l} + \frac{We_s}{We_l}\frac{1}{h^3} \tag{A.21}$$

$$E_4 = \frac{(-\mathrm{i}\bar{\omega} + \mathrm{i}\bar{k})^2 I_o(\bar{k}h)}{\bar{k} l_{18} I_1(\bar{k}h)} l_{17} - \frac{2\mathrm{i}\bar{k}^2 (-\mathrm{i}\bar{\omega} + \mathrm{i}\bar{k})^2}{\bar{k} l_{13}} K_o(\bar{k}h) l_{15} + \frac{2Z(-\mathrm{i}\bar{\omega} + \mathrm{i}\bar{k})\bar{k} I_1'(\bar{k}h)}{l_{18} I_1(\bar{k}h)} l_{17} + \frac{4\bar{Z}\bar{k}^3 \mathrm{i}(-\mathrm{i}\bar{\omega} + \mathrm{i}\bar{k}) K_1'(\bar{k}h)}{l_{13}} l_{15} \tag{A.22}$$

$$E_5 = -\frac{4Z\bar{k}^2 (-\mathrm{i}\bar{\omega} + \mathrm{i}\bar{k})\bar{s} I_1'(\bar{s}h) l_{10} l_9}{l_9 l_{11}} - \frac{4\bar{Z}\bar{k}^2 (-\mathrm{i}\bar{\omega} + \mathrm{i}\bar{k})\bar{s} K_1'(\bar{s}h)}{l_{11}} l_9 \tag{A.23}$$

$$F_1 = -\frac{(-\mathrm{i}\bar{\omega} + \mathrm{i}\bar{k})^2}{\bar{k} l_{18} I_1(\bar{k}h)} I_o(\bar{k}) l_{16} + \frac{2\mathrm{i}\bar{k}^2 (-\mathrm{i}\bar{\omega} + \mathrm{i}\bar{k})^2}{\bar{k} l_{13}} K_o(\bar{k}) I_1(\bar{k}) l_{14} - \frac{2Z(-\mathrm{i}\bar{\omega} + \mathrm{i}\bar{k}) I_1'(\bar{k})\bar{k} l_{16}}{l_{18} I_1(\bar{k}h)} - \frac{4Z\bar{k}^3 (-\mathrm{i}\bar{\omega} + \mathrm{i}\bar{k}) K_1'(\bar{k})}{l_{13}} I_1(\bar{k}) l_{14} \tag{A.24}$$

$$F_2 = -\frac{4Z\bar{k}^2 (-\mathrm{i}\bar{\omega} + \mathrm{i}\bar{k})\bar{s} I_1'(\bar{s}) I_1(\bar{k}) l_{12}}{l_9 l_{11}} + \frac{4Z\bar{k}^2 (-\mathrm{i}\bar{\omega} + \mathrm{i}\bar{k})\bar{s} K_1'(\bar{s})}{l_{11}} l_6 l_4 l_1(\bar{k}) \tag{A.25}$$

$$F_3 = -\frac{(-\mathrm{i}\bar{\omega}+\mathrm{i}\bar{k})^2 I_o(\bar{k})}{\bar{k} l_{18} I_1(\bar{k}h)} l_{17} - \frac{2\mathrm{i}\bar{k}^2(-\mathrm{i}\bar{\omega}+\mathrm{i}\bar{k})^2}{l_{13}\bar{k}} K_o(\bar{k}) l_{15} - \frac{(-\bar{\omega}+\bar{k}\sqrt{(We_o/We_l)(1/g_o)})^2 g_i K_o(\bar{k})}{\bar{k} K'_o(\bar{k}h)} + \frac{2Z(-\mathrm{i}\bar{\omega}+\mathrm{i}\bar{k})\bar{k} I'_1(\bar{k})}{l_{18} I_1(\bar{k}h)} l_{17} \quad (A.26)$$

$$F_4 = \frac{4Z\bar{k}^3 \mathrm{i}(-\mathrm{i}\bar{\omega}+\mathrm{i}\bar{k}) K'_1(\bar{k})}{l_{13}} l_{15} - \frac{4Z\bar{k}^2(-\mathrm{i}\bar{\omega}+\mathrm{i}\bar{k})\bar{s} I'_1(\bar{s}) l_{10} l_9}{l_9 l_{11}} - \frac{4Z\bar{k}^3(-\mathrm{i}\bar{\omega}+\mathrm{i}\bar{k})\bar{s} K'_1(\bar{s})}{l_{11}} l_9 \quad (A.27)$$

$$F_5 = \frac{1}{We_l}(1-\bar{k}^2) - \frac{We_{so}}{We_l} + \frac{We_s}{We_l} \quad (A.28)$$

$$\frac{G}{H} = -\frac{E_4+E_5}{E_1+E_2+E_3} \quad (A.29)$$

$$\frac{G_1}{H_1} = -\frac{F_3+F_4+F_5}{F_1+F_2} \quad (A.30)$$

References

[1] A.H. Lefebvre, Atomization and Sprays, Hemisphere, New York, 1989.

[2] R. Robitaille, J.F. Pariseau, F.A. Leblond, M. Lamoureux, Y. Lepage, J.P. Hallé, Studies on small (<350 μm) alginate-poly-L-lysine microcapsules. III. Biocompatibility of smaller versus standard microcapsules, J. Biomed. Mater. Res. 44 (1999) 116–120.

[3] G. Orive, R.M. Hernández, A.R. Gascón, M. Igartua, J.L. Pedraz, Development and optimisation of alginate-PMCG-alginate microcapsules for cell immobilisation, Int. J. Pharm. 259 (2003) 57–68.

[4] S. Sugiura, T. Oda, Y. Izumida, Y. Aoyagi, M. Satake, A. Ochiai, N. Ohkohchi, M. Nakajima, Size control of calcium alginate beads containing living cells using micro-nozzle array, Biomaterials 26 (2005) 3327–3331.

[5] E. Giffen, A. Muraszew, The Atomization of Liquid Fuels, John Wiley, New York, 1953.

[6] N. Chigier, Energy Combustion and the Environment, McGraw-Hill, New York, 1981.

[7] R.L. Panton, Incompressible Flow, John Wiley and Sons, Inc., New York, 1995.

[8] M. Adelberg, Breakup rate and penetration of a liquid jet in a gas stream, AIAA J. 5 (1967) 1408–1415.

[9] M. Adelberg, Mean drop size resulting from the injection of a liquid jet into a high-speed gas stream, AIAA J. 6 (1968) 1143–1147.

[10] H. Jeffreys, On the formation of water waves by wind, Proc. R. Soc. London A 107 (1925) 189.

[11] E. Mayer, ARS J. 31 (1961) 1783–1785.

[12] E.P. Herrero, E.M.M. Del Valle, M.A. Galán, Development of a new technology for the production of microcapsules based in atomization processes, Chem. Eng. J. 117 (2006) 137–142.

[13] E.P. Herrero, E.M.M. Del Valle, M.A. Galán, Modelling prediction of the microcapsule size of polyelectrolyte complexes produced by atomization, Chem. Eng. J. 121 (2006) 1–8.

[14] Y. Jia, Y. Kanno, Z.-p. Xie, New gel-casting process for alumina ceramics based on gelation of alginate.

[15] N.K. Rizk, H.C. Mongia, Model for air blast atomization, J. Propul. Power 7 (1991) 305–311.

[16] J. Shen, X. Li, Instability of an annular viscous liquid jet, Acta Mech. 114 (1996) 167–183.

[17] X. Li, R.S. Tankin, On the temporal instability of a two-dimensional viscous liquid sheet, J. Fluid Mech. 226 (1991) 425–443.

[18] Y. Liao, S.M. Jeng, M.A. Jog, Advanced sub-model for air blast atomizers, J. Propul. Power 17 (2001) 411–417.

[19] F. Chen, J.Y. Tsaur, F. Durst, K. Samir, On the axisymmetry of annular jet instabilities, J. Fluid Mech. 488 (2003) 355–367.

[20] L.G. Sarasua, A.C. Sicardi, Viscosity influence on the stability of a swirling jet with nonrotating core, Phys. Fluids 12 (2000) 1607–1610.